Three-Dimensional Printing of Layered Machinable Ductile Carbide

D. J. D'Costa[(1)], S. D. Dimovski[(1)], F. Lin[(1)], T. El-Raghy[(2)], M.W. Barsoum[(2)] and W. Sun[(1)]
[(1)]Department of Mechanical Engineering and Mechanics
[(2)]Department of Materials Engineering
Drexel University, Philadelphia, PA 19104

Abstract

Ti_3SiC_2 carbide represents a new class of ceramics with excellent electrical and mechanical properties. This paper presents our preliminary studying on using 3D printing technique, combining with cold isostatic pressing and sintering processing to prototype Ti_3SiC_2 carbide components. The basic mechanical, electrical and thermal properties of Ti_3SiC_2 carbide material will be reviewed. Results in die and mold-free 3D printing processing of Ti_3SiC_2 carbide prototyping will be reported. The SEM characterization of the prototypes and the correlation with the processing parameters will be presented.

Keywords: Ductile carbide ceramics, manufacturing, freeform fabrication, 3D printing.

1. Introduction

Modern engineering practice has proved that solid freeform fabrication is a fast and reliable process to turn the conceptual design into 3D prototypes [1]. Recently, more and more research interests have been put on using freeform fabrication techniques to directly prototype functional ceramic part in order to obtain more freedom for design geometry (shape) of ceramic structure. If obtainable by this technology, ceramic parts are expected to have lower cost since the process can be highly automated and there are also additional energy and material savings. Besides, most of the ceramics are very difficult to machine therefore this process can significantly widen the application of certain ceramic materials.

Some of reported rapid prototyping technology involve the use of a jet printer, wherein a ceramic ink is used in a pressurized continuous ink jet printer which deposits the ceramic and ink mixture according to the inputted CAD mode [2, 3], finally leading to the development of the ceramic prototype. The technology of 3D printing has also been used in the generation of prototypes, leaning on the techniques such as: spraying down of the ceramic slurry [4], multiple layer tape casting and printing slurry through a nozzle [5]. Another process that is developed is known as robocasting [6] - a computer aided deposition of highly concentrated ceramic colloidal slurries to directly form complex shapes without the use of molds or dies. Established freeform fabrication techniques such as Extrusion Free Form and Fused Deposition Modeling [7] uses the principle of deposition of feedstock layer by layer until the final part is fabricated. Inkjet printing of electroceramic lead zirconate titanate by ink jet printing (using a piezoelectric actuator to eject the ink) produces a 3D part using overprinting technique [8]. The 3D printing technique of electronic ceramic components employs deposition of a slurry bed by a slurry jet, curing the bed using IR radiation, printing a 2D image using a binder jet and repeating the procedure in sequence to produce the final 3D part. The part is then immersed in a sonicated water bath to remove the unprinted binder layers and the final part is isolated [9]. Electrophotographic powder deposition [10] technique employs the deposition of charged powder particles layer-by-layer, resulting in the precise deposition of particles to the desired shape. Electromagnetic ink jet printing employs the ejection of ceramic inks via a electromagnetic valve printing head [11], this process is repeated to get the final

desired part. Dispersion of ceramic inks using an ultrasonic horn uses the principle of ultrasonic vibration to disperse the ink layer by layer to form the final 3D object [12].

This paper will report our preliminary results of using Z402 3D Printing technique to prototype Ti_3SiC_2 carbide components. The objective of this research is to explore the feasibility of using 3D Printing technology in the freeform fabrication of new invented Ti_3SiC_2 carbide material. The presentation of this paper is outlined as following. The properties of Ti_3SiC_2 carbide material is reviewed in Section 2. The 3D Printing process with post-processes of cold isostatic pressing and sintering is described in Section 3. Results and SEM characterization of the available prototyping samples and the correlation with the processing parameters is discussed in Section 4. Summary, conclusion and discussions are presented in Section 5.

2. Properties of novel Ti_3SiC_2 carbide

Polycrystalline bulk samples of Titanium Silicon carbide Ti_3SiC_2 were synthesized by reactively hot pressing Ti, graphite and SiC powders at a pressured elevate temperature. This newly invented Ti_3SiC_2 carbide has superior mechanical, electrical and thermal properties [13-17]. Laboratory results reveal that Ti_3SiC_2 carbide is a ceramic having remarkable properties such as good electrical conductivity that is twice that of pure Titanium. The thermal expansion coefficient, the ambient temperature thermal conductivity, and heat capacity are roughly twice that of pure Titanium, respectively. Its density is roughly half the density but almost double the stiffness of Nitrogen-based super alloys. Ti_3SiC_2 is relatively soft with Vickers hardness of 2-5 GPa and Young's Modulus of 320 GPa, but elastically stiff and easily machinable. Ti_3SiC_2 retains these mechanical properties at high temperatures and is stable at high temperature of 1800°C with excellent high temperature mechanical properties. When heated to 1400°C and quenched, this ceramic actually increases in strength, wherein other ceramics will have a drastic reduction in strength when subjected to the same conditions of quenching. In addition, Ti_3SiC_2 is self-lubricating with one of the lowest kinetic friction coefficients of $2^{-5} \times 10^{-3}$.

One remarkable property of Ti_3SiC_2 carbide is its ease machinablility, in spite of its high stiffness. The layered structure of material and its ductility contributes to direct machinability to close tolerances, whereas in other cases the ceramic needs to be sintered after machining which results in an additional shrinkage of 2%. Ti_3SiC_2 is the only carbide that can be cut manually using a hacksaw. Because of the good electrical properties it is also easily shaped and cut using Electric Discharge Machining.

Low material cost, good thermal conductor, good thermal shock resistance and chemical resistance, stable mechanical and electrical properties at high temperature, and its machinability greatly contribute to the development of various applications of this ceramic. The physical, thermal, electrical and mechanical properties of Ti_3SiC_2 are summarized in the Appendix 1.

3. 3D Printing of Ti_3SiC_2 carbide component

Flow chart of the process used for prototyping Ti_3SiC_2 carbide components is shown in Figure 1. The prototyping of Ti_3SiC_2 carbide components was divided into three processes: 1) rapid prototyping

process, 2) cold isostatic pressing process, and 3) sintering process. In the rapid prototyping process, the components were fabricated by using Z402 3D Printing System (Z-Corp). The components were designed as solid model files and then converted to STL files for system slicing. The 3D Printing System stacks the slices to construct the green part.

The Z402 consists of a feed bay, a build bay, and a binder spray head with cartridge. The slice data obtained from the build file is inputted to the machine. The binder spray head initially sprays the binder on to the first powder layer (depending on the cross-section of the green part at that particular section). As the binder head moves across the 2 bays, it rolls a layer of powder (depending on the specified layer thickness) from the feed bay to the build bay. This process continues, layer by layer, until the entire model has been built. The green part is allowed to cure in the build bay for about 1 hour before removal for further post prototyping processing.

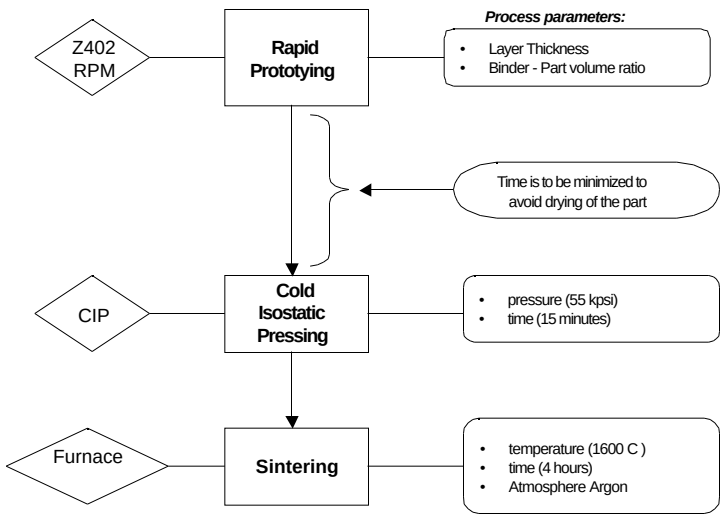

Figure 1: 3D fabrication process of Ti_3SiC_2 carbide parts

There are two main processing parameters we are interested in the prototyping process, namely, 1) layer thickness, ranging from 0.0035” to 0.05” for every layer built, and 2) binder concentration, ranging being 2% to 40%. For the green parts built with Ti_3SiC_2 carbide, we have varied the binder concentration as 10%, 20% and 30%. The 3D Printing processing parameters are summarized in Table 1.

Table 1: 3D Printing machine specifications and process parameters

Primary specifications governing the prototype	
Base material (powder)	Ti_3SiC_2 carbide
Binder (water based)	zb-7
Layer thickness	Range is from 0.05” to 0.0035”
Binder saturation	Shell / Core (percentage volume fraction) Range is from 2% to 40%
Build speed Accuracy	1” / hour along z-axis 0.5% along X-Y axes, 1% along Z-axis

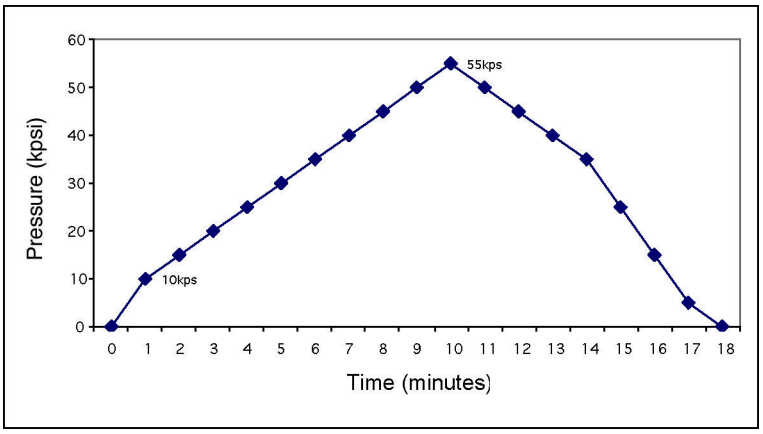

Figure 2: Cold isostatic pressing pressure application profile

After the green part is built, it is placed inside a vacuum-sealed plastic bag and subjected to a cold isostatic pressure. The pressure application profile is shown in Figure 2. The pressure increases from 0 kpsi to 55 kpsi and then gradually decreases to 0 kpsi for a total duration of about 20 minutes. The pressed green part is further subjected to sintering in a furnace to a temperature of 1600°C for a period of 4 hours in Argon atmosphere. The Sintering temperature application profile is shown in Figure 3.

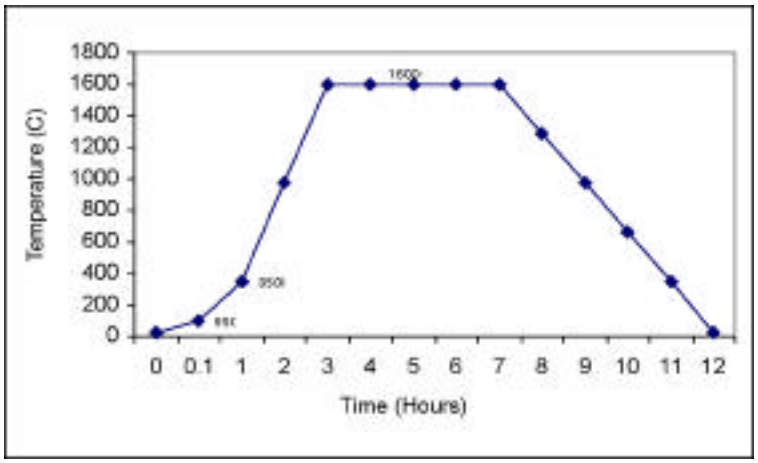

Figure 3: Sintering temperature application profile

Ti_3SiC_2 carbide powder (40 μm particle size) is used for 3D printing of 1” x 1” x 0.4” samples. Layer thickness and binder concentration were varied. Samples were made for two different layer thickness, 0.0035” and 0.007”. Amount of binder was varied as 30%, 20% and 10% in order to understand the effect of binder concentration on the microstructure and porosity of the green part.

To understand the effect of cold isostatic pressing (CIP) on the structural properties of the components, we processed two sets of samples. One set of samples were subjected to CIP, then sintered after 3D printing. While the other set were sintered directly without CIP process (Figure 4). Both sets were cut and standard procedure was used to prepare samples for microstructure characterization by optical microscope and SEM. Optical microscope is used to measure surface densities for each sample. Supporting software provides threshold and density slice tools by which percentage of black and white phases can be measured directly. An average density for each sample is calculated as a mean value for the

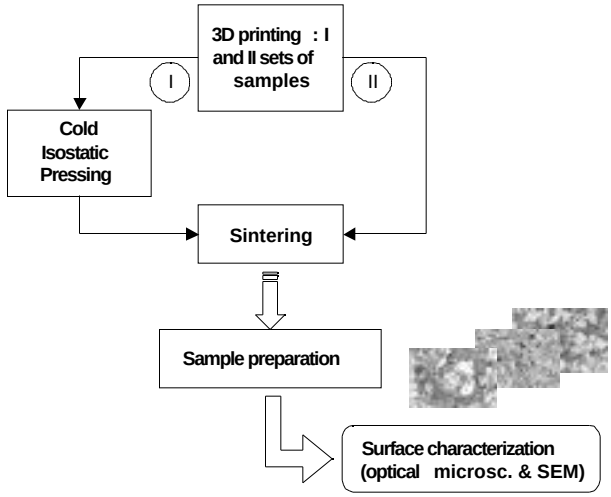

Figure 4. Experimental procedure flow-chart

data retrieved by random choice of at least 25-30 points on each sample. Microphotographs were captured by both: optical and SEM microscopes.

4. Results and SEM characterization

The experiment was conducted by fabricating simple green parts with varying binder concentration and layer thickness and subjecting the parts to two independent post processes. One set of green parts was subjected to both CIP and sintering and the other set was subjected to only sintering without CIP.

Green parts of simple shape (rectangular cuboids) were successfully prototyped and produced by a 3D printing machine. Samples subjected to CIP need to be freshly generated in order to retain the shape of the part without being damaged in the process of transferring form the 3D printing machine to the CIP device. Traces of moisture mixed with ceramic powder were found inside the sealed plastic packaging, indicating that, under the CIP process, certain amount of binder was squeezed out of the part. It is also observed that the shrinkage was higher in the case of parts subjected to CIP and sintering than in the case of without CIP process. In the former the average shrinkage was observed to be 20%, while in the latter it was 12%. This further suggests that a large amount of porosity may stay in the samples if not subjected to the CIP process. Results of the Ti_3SiC_2 carbide density for processes with CIP and without CIP for different binder concentration and layer thickness are summarized in Table 2.

Table 2: Ti_3SiC_2 carbide densities at different processing parameters

Binder Concentration (%)	Layer Thickness (inches)	Density (CIP and Sintering) (%)	Density (Sintering without CIP) (%)
10	0.007	94.33	65.54
20	0.0035	93.39	60.18
30	0.0035	79.44	55.89

From the results it is very clear that there is a significant effect of both process parameters and the process methods on the density of the Ti_3SiC_2 carbide components. From Figure 6, we observe that at the same binder concentration, there is a substantial increases in density of about 15% in the case of the green part being subjected to CIP and sintering, and an increase of about 10 % in the sintering without CIP process. An average increase of 28% in density is observed when the green parts are subjected to the CIP and sintering process compared with the sintering without CIP process when the binder concentration is decreased from 30% to 10%.

Three sets of samples were examined and results were reported in Figure 6. First set of samples had a 30% binder concentration, subjected to CIP and without CIP then sintered for 4 hours at 1600°C temperature in Argon atmosphere. Density was measured to be about 80% with CIP and sintering and 56% without CIP and sintering. At this density range, the components may not be suitable for structural ceramics that generally requires a density above 90%. The samples with 20% binder concentration (with and without CIP) were exposed to the same sintering parameters, and ended up with increased density. The part with 20% binder concentration after CIP and sintering resulted in a density of over 93%, very close to the required density of structural ceramic materials. Without CIP, the density at 20% binder concentration was dropped to about 60%. For samples with 10% binder concentration, we obtained that the density of about 94% for Ti_3SiC_2 carbide components with CIP and 65% without CIP process. Therefore, CIP process contributes significantly to increase the density of the prototyped components.

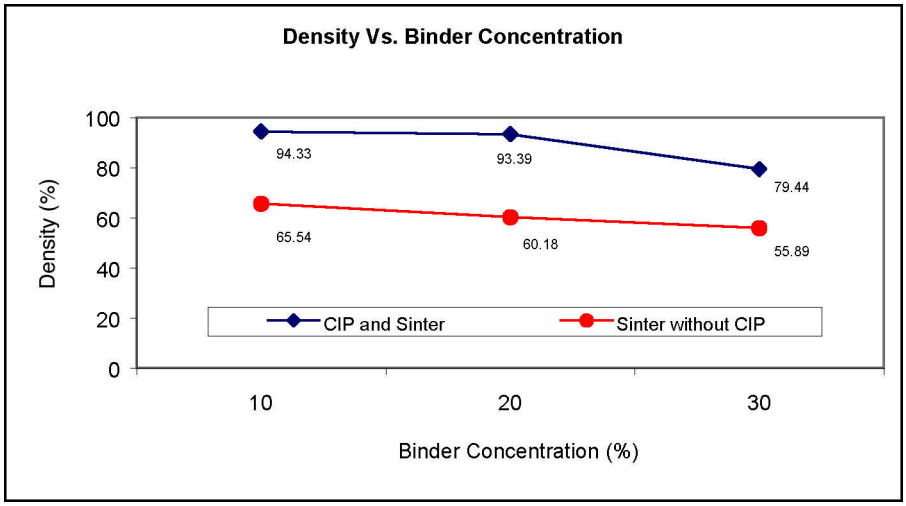

Figure 6: Density variation vs. different processes and processing parameters

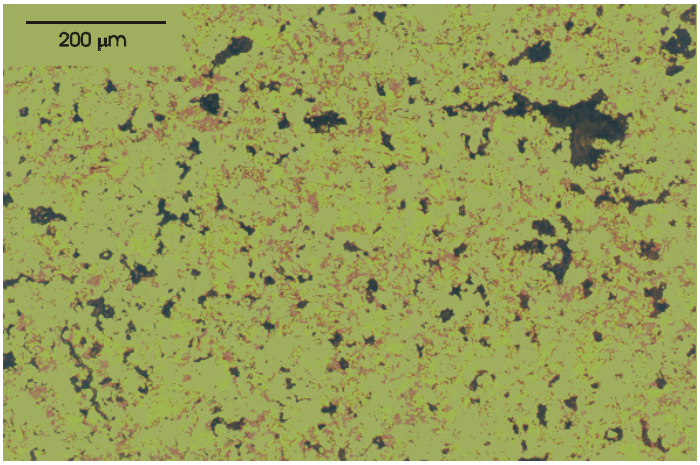

Figure 7: Optical microscopy of Ti_3SiC_2 carbide at 100 times magnification (Binder concentration of 20% with CIP)

Another parameter that can have influence on porosity formation is layer thickness. Layer thickness can directly affect distribution of the flaws since it affects uniformity of powder packing. Currently, we do not have enough data available for concluding the effect of layer thickness on porosity, flaw size and density of the Ti_3SiC_2 carbide components.

Figure 7 presents a optical microscope microphotograph of Ti_3SiC_2 carbide sample with 20% binder concentration at x100 magnification. Uniform structure, grain size and grain distribution of Ti_3SiC_2 is observed. From this we can observe that sintering reaction was not completed in full since the white phase of TiC and gray phase of SiC is still distinguishable within the structure of Ti_3SiC_2 grains.

For the sake of comparison, microphotographs at x200 (80 μm) and x500 (40 μm) magnification for two different samples obtained by optical microscope are presented in Figure 8.a-d. Flaws are clearly distinguishable.

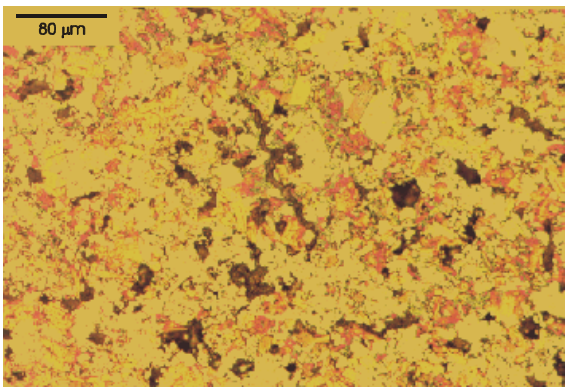

a. 20% binder concentration with CIP

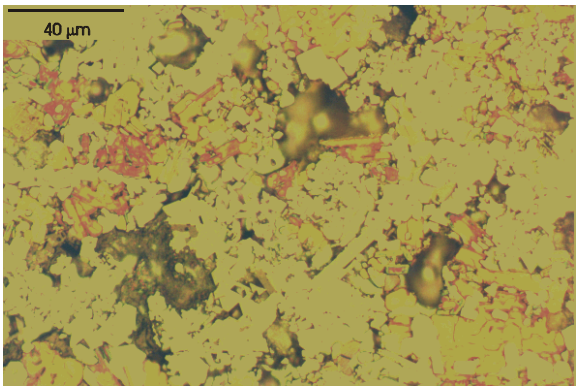

b. 20% binder concentration with CIP

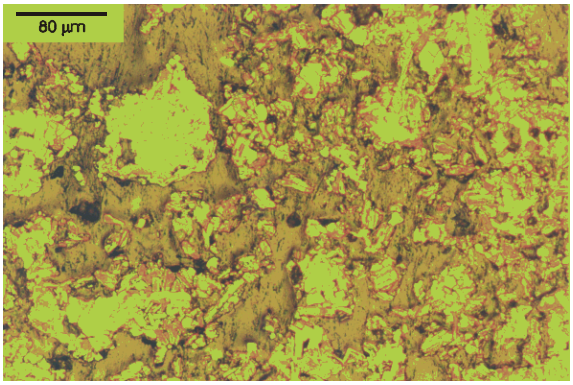

c. 10% binder concentration w/o CIP

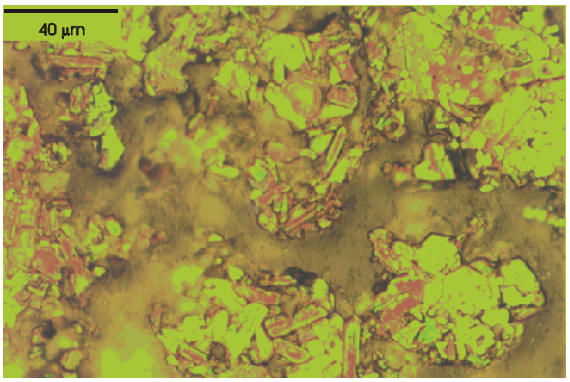

d. 10% binder concentration w/o CIP

Figure 8: Optical microscopy of Ti_3SiC_2 carbide at x200 and x500 magnification respectively
a - b. 20% binder concentration samples with CIP
c - d. 10% binder concentration samples without CIP

Figure 8a. is obtained for the sample with 20% binder concentration that was exposed to CIP and sintered. It shows flaws near the surface formed during processing. Flaw distribution is appeared to be uniform and the shape is mostly spherical. In some areas, mostly concentrated closer to the surface the flaws are linked into the cracks. It is highly probable that these cracks appeared during the manipulation of green parts before CIP and sintering while the parts are still weak. The same sample at the higher magnification is shown in Figure 8b. The pileups of TiC and SiC grains are observable around the small

and rather smooth flaws. These two separate phases are present because reaction of forming Ti_3SiC_2 is not completed. For 10% binder concentration sample that was not exposed to CIP highly porous structure is observable, as shown in Figure 8c. Most of the TiC and SiC was gone during sintering due to almost the full reaction, but since the sample was not exposed to CIP, a quite poor structure with lots of flaws and cracks was achieved and can be observed in Figure 8d.

Series of Optical microscopiess with different magnifications for Ti_3SiC_2 carbide at 10% binder concentration with CIP process are presented in Figure 9. For x50 magnification the isolated flaws are observed within the sample. Separate phases are also present and are due to presence of impurities in the material. For x100 magnification more obvious separated flaws with few of them converging into one microcrack are observed.

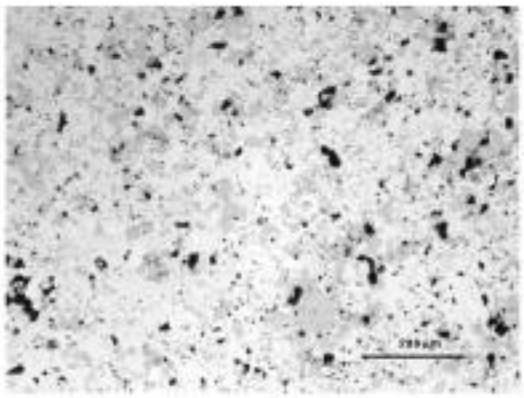

a. x100 (200 μm) magnification

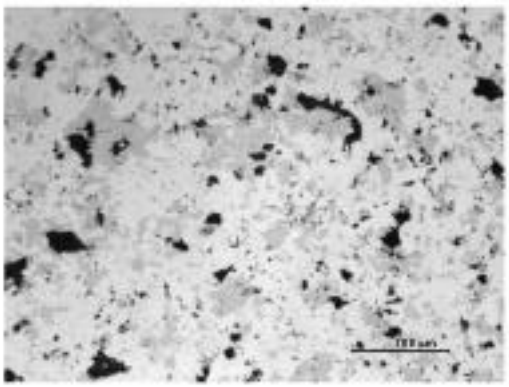

b. x200 (100 μm) magnification

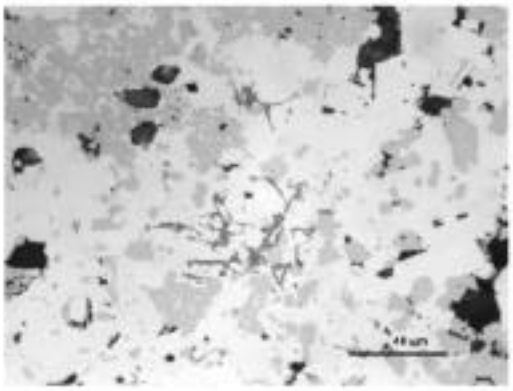

c. x500 (40 μm) magnification

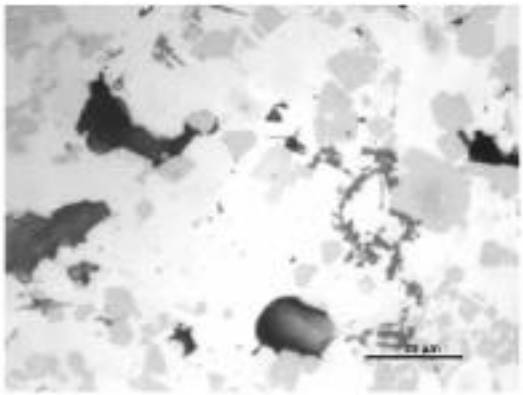

d. x1000 (20 μm) magnification

Figure 9: Optical microscopiess of Ti_3SiC_2 carbide 10% binder concentration samples with CIP

An interesting microphotograph of uncompleted reaction is shown in Figure 10. Clearly distinguishable grains of TiC and SiC are mixed with Ti_3SiC_2 grains around a crack.

SEM microphotograph of the same sample with the 93% density is captured at 1500 times magnification and presented in Figure 11. Small white grains of TiC are distinguishable within the large laminated grains of Ti_3SiC_2. This and the previous few microphotographs suggest that the final density of the structure and its quality is predominantly governed by CIP and sintering process, and less affected by the binder concentration, particularly if the binder concentration is small, since the most of the binder already dry out even before the sintering reaction started.

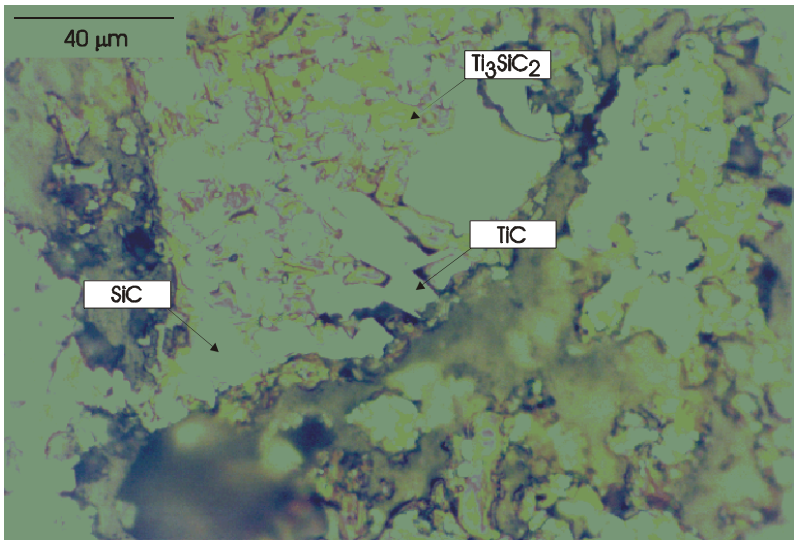

Figure 10: Unaccomplished reaction in 20% binder concentration sample

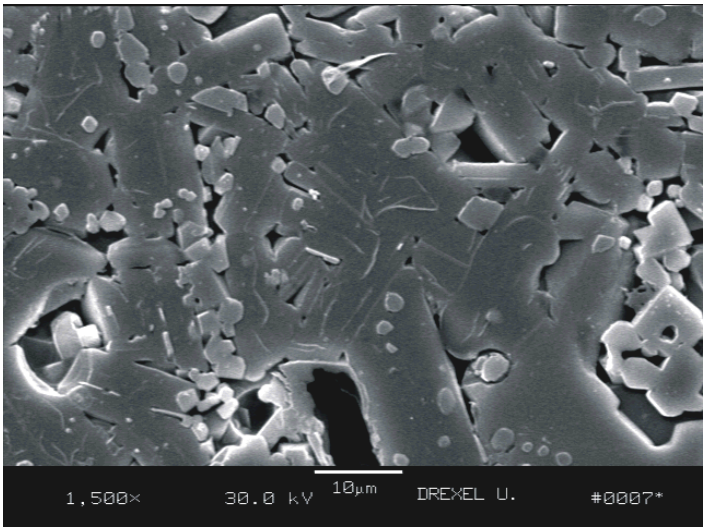

Figure 11: SEM microphotograph of 20% binder concentration samples after CIP and sintering

5. Summary and Conclusion

This paper presents our preliminary results of investigation on the feasibility of using 3D printing technology to produce functional components from a novel Ti_3SiC_2 structure ceramic material. Current results prove that the method can be used to fabricate ceramic structures having a density of the order of 90% and above. At this stage of research the following observations and conclusions can be made:

- Variation of the binder concentration within the certain range does affect the structural quality of the prototyped components. In general, the minimization of the binder concentration will reduce the porosity, or increase the density of the components after sintering. However, it is observed that the green part will not sinter very efficiently if the binder concentration is too high, and the porosity will not change if the binder concentration is too lower;
- Cold isostatic pressing has a significant influence on the density of the prototyping components;

- Minimizing the time between prototyping and CIP can retain green part strength, i.e. CIP should be done immediately after prototyping, when the part is fresh. Natural or heat drying of the green part after prototyping will result in a substantial loss in binder as a result of which the part will not retain sufficient strength for post prototyping processes;

Future work of this research is to conduct a systematic study on the processing mechanics of 3D printing in fabricating Ti_3SiC_2 carbide structure. This will include a series of studies on the structural formability and the effect of the processing parameters on part quality and microstructural properties. Standard structural sample of the Ti_3SiC_2 carbide will be produced by use of 3D printing system. Other than elastic mechanical properties, its creep, fatigue and fracture toughness will also be examined. The machinability of the Ti_3SiC_2 carbide will also be studied.

References

1. J. G. Heinrich: "New developments in the solid freeform fabrication of ceramic components", *Ceramic Forum International*, Vol. 76, No. 5, 1999, pp. 29-35
2. P.B. Blazdell, J.R.G. Evans: "Application of continuous ink jet printer to solid freeforming of ceramics", *Journal of Materials Processing Technology*, Vol. 99, 2000, pp. 94-102
3. M. Mott, J.-H. Song and J. Evans: "Microengineering of ceramics by direct ink-jet printing", *Journal of American Ceramics Society*, Vol. 82, No. 7, 1999, pp. 1653-58.
4. J. Moon, J. Grau, P.J. Baker, M. Caradonna, M.J. Cima: "Binder-powder bed interactions in the slurry-based 3-dimensional printing process", Conference on freeform fabrication, 1997.
5. J. Grau, J. Moon, M.J. Cima: "Structural ceramics fabricated by 3-dimensional printing", Conference on freeform fabrication, 1997.
6. J. Cesarano, "Robocasting: Direct fabrication of ceramicssss from colloidal suspensions", Conference on freeform fabrication, 1997.
7. A. Bandyopadhyay, C.Daai, G. Qqi, M. Agarwala, S. Rangarajan, A. Safari, N. Langrana, S.C. Danforth, V.Jamalaabad, R. van Weeren, P.J. Whalen: Development and optimization of fused deposition of ceramics for structural silicon nitride components", Conference on freeform fabrication, 1997.
8. J. Windle, B. Derby: "Ink jet printing of PZT aqueous ceramic suspensions", *Journal of Materials Science Letters*, Vol. 18, 1999, pp. 87-90
9. S. Uhland, R. Holman, B. DeBear, P. Saxton, M. Cima, E. Sachs, Y. Enokido and H. Tsuchiya: "Three-dimensional printing, 3DP^{TM}, of electronic ceramic components", *Proceedings of Solid Freeform Fabrication Symposium*, 1999, pp. 865-872.
10. A.V. Kumar and H. Zhang: "Electrophotographic powder deposition for freeform fabrication", Solid Freeform Fabrication Symposium, 1999, pp. 647-653
11. M.J. Wright, R.G. Evans: "Ceramic deposition using an electromagnetic jet printer station", *Journal of Materials Science Letters*, Vol. 18, 1999, pp. 99-101
12. H. Rashid, B.Y. Tay, M.J. Edirisinghe: "Dispersion of ceramic ink using an ultrasonic disruptor", *Journal of Materials Science Letters*, Vol. 19, 2000, pp. 799-801
13. T. El-Raghy, M. W. Barsoum and M. Radovic: "A layered machinable ductile carbide", in press
14. T. El-Raghy, M. W. Barsoum, A. Zavaliangos and S. R. Kalidindi: "Processing and mechanical properties of Ti_3SiC_2, Part II: Mechanical properties", *Journal of American Ceramics Society*, Vol. 82, 1999., pp. 2855-60.
15. T. El-Raghy and M. W. Barsoum: "Processing and mechanical properties of Ti_3SiC_2, Part I: Reaction Path and Microstructure Evolution", *Journal of American Ceramics Society*, Vol. 82, 1996., pp. 1953-56.
16. M. Radovic, M. W. Barsoum, T. El-Raghy, J. Seidensticker and S. Wiederhorn: "Tensile Properties of Ti_3SiC_2 in the 25-1300 °C temperature range", *Acta materialia*, in press
17. T. El-Raghy and M. W. Barsoum: "Synthesis and Characterization of a Remarkable Ceramic: Ti_3SiC_2", *Journal of American Ceramics Society*, Vol. 79, No. 7, 1999, pp. 1653-58.

Appendix:

Table 1: Summary of physical, thermal, and electric properties of Ti_3SiC_2 [13]

Property	Temper.	Value	Comments
Structure and Physical Properties			
Mol. wt.	RT	195.78 gm/mol	
Structure		Hexagonal, $P6_3/mmc$	
Lattice parameters	RT	a = 0.3068±0.002 nm b = 1.7669±0.006 nm	
Unit cell volume	RT	1.4348×10^{-28} m^3	
Theoretical Density	RT	4.53 g/cm^3	
Molar vol.		43 cm^3/mol	
Thermal Properties			
Thermal Exp.	25-1200 °C	$(9.1\pm0.2) \times 10^{-6}$ K^{-1}	Bulk dilatometric
α_a α_c	25-1000 °C	$(8.6 \pm0.1) \times 10^{-6}$ K^{-1} (9.7±0.1) x c	HT neutron diffraction. Anisotropy in TCE's is mild (≈Al_2O_3)
Thermal Conductivity	25-1200 °C 25-1200 °C	37 W/m K 38.6-0.0045 T (K)	≈ 90 % of heat is conducted by electronic defects
Heat Capacity	25°C 25-1200 °C	110 J/ mol K 164.4 – 16419/T (K)	Heat capacity is ≈ 3 times that of stoichiometric TiC
Debye Temp.		715 K 670 K 780 K	Low temperature heat capacity High temp. neutron diffract. Acoustic
Electrical Properties			
Resistivity & its temp. depend.	25°C	0.22 μΩ m 0.11 μΩ m	At 0.22 resistivity is ≈ _ that of Ti metal
	77-300 K	$\rho/\rho_{RT} = 1+0.004(T(K)–300)$	Resistivity increases linearly with increasing temperature
Elastic properties			
Young's modulus	25°C	332-333 GPa $E/E_{RT}=1-0.95 \times 10^{-4}$ ΔT	It is the stiff as Mo or Si_3N_4 and yet is readily machinable
Shear modulus	25°C 25°C 77-300 K	134-139 GPa $\mu/\mu_{RT} = 1-1.4 \times 10^{-4}$ ΔT	The sear modulus decreases linearly with increasing temperature
Bulk modulus	25°C	185 GPa 206 GPa	Calculated from E, G and ν. Direct measurement (XRD)
Poisson's ratio	25°C	0.2	
Chemical properties			

Parabolic oxidation rates	1000°C 1240°C 1400°C	1.3×10^{-8} ($Kg^2m^{-4}s^{-1}$) 3×10^{-6} 1×10^{-4}	Protective oxides that form TiO_2 and SiO_2 are resistant to thermal cycling. At 1000°C oxidation rate is comparable to Cr metal.

Table 2: Summary of mechanical properties of Ti_3SiC_2 [13]

Property	Temper.	Value	Grain size	Comments
Hardness and ultimate stresses				
Hardness	RT	4 GPa 4 GPa	3-5 μm 100-300 μm	
Ultimate compressive stresses	RT 1000°C 1300°C	100 MPa 900 MPa 420 MPa	3-5 μm	The values listed were measured at a strain rate of 10^{-4} s^{-1}.
	RT 1000°C 1300°C	720 MPa 600 MPa 300 MPa	100-300 μm	The values listed were measured at a strain rate of 10^{-4} s^{-1}.
Ultimate tensile stresses	RT 1000°C 1100°C 1200°C 1300°C	223 MPa 125 MPa 123 MPa 60 Mpa 12 MPa	3-5 μm	The values one obtains are strong function of strain rate. The values listed here were measured at a strain rate of ≈ 1.4×10^{-4} s^{-1}. Above 1200°C strains to failure > 5%.
Creep properties				
Creep rates at 20 MPa	1000°C 1200°C	1×10^{-8} 2×10^{-6}	3-5 μm	Act. energy for creep is 420 kJ/mol. Stress exponent is ≈ 1.5
Creep rates at 40 MPa	1000°C 1200°C	1.5×10^{-8} 1.1×10^{-5}	3-5 μm	
Fatigue and fracture toughness				
Fatigue thresholds	RT	6 MPa√m 8 MPa√m	3-5 μm 100-300 μm	The fatigue curves are very steep and extrapolate to the thresholds listed.
Fatigue toughness	RT RT RT RT	8 MPa√m 9.5 MPa√m 8-11 MPa√m 14-16 MPa√m	3-5 μm 3-5 μm 100-300 μm	Initial fracture toughness Final fracture toughness Initial fracture toughness Final fracture toughness
Wear resistance				
Sliding wear rate (440 S. steel)	RT RT	4.25×10^{-3} (mm^3/Nm) 1.34×10^{-3} (mm^3/Nm)	3-5 μm 100-300 μm	Wear resistance of fine-grained material is worse than coarse-grained. Coefficient of friction is high (0.82) because of third body abrasion.